Atmos. Meas. Tech. Discuss., 3, 1163–1196, 2010
www.atmos-meas-tech-discuss.net/3/1163/2010/

Atmospheric Measurement Techniques Discussions

This discussion paper is/has been under review for the journal Atmospheric Measurement Techniques (AMT). Please refer to the corresponding final paper in AMT if available.

Improved ozone profile retrieval from spaceborn UV backscatter spectrometers

B. Mijling, O. N. E. Tuinder, R. F. van Oss, and R. J. van der A

Royal Netherlands Meteorological Institute (KNMI), P.O. Box 201, 3730 AE, De Bilt, The Netherlands

Received: 12 February 2010 – Accepted: 15 March 2010 – Published: 25 March 2010

Correspondence to: B. Mijling (mijling@knmi.nl)

Published by Copernicus Publications on behalf of the European Geosciences Union.

Abstract

The Ozone Profile Algorithm (OPERA), developed at KNMI, retrieves the vertical ozone distribution from nadir spectral satellite measurements of back scattered sunlight in the ultraviolet and visible wavelength range. To produce consistent global datasets the algorithm needs to have good global performance, while short computation time facilitates the use of the algorithm in near real time applications.

To test the global performance of the algorithm we look at the convergence behaviour of the ozone retrievals, based on the data of the GOME instrument (on board ERS-2) for February and October 1998. In this way, we uncover different classes of retrieval problems, related to the South Atlantic Anomaly, low cloud fractions over deserts, desert dust outflow over the ocean, and the intertropical convergence zone. The influence of external input data including the ozone cross-sections and the ozone climatologies on the retrieval performance is also investigated. By using a priori ozone profiles which are selected on the expected total ozone column, retrieval problems due to anomalous ozone distributions (such as in the ozone hole) can be avoided.

By applying the algorithm adaptations the convergence statistics improve considerably, not only increasing the number of successful retrievals, but also reducing the average computation time, due to less iteration steps per retrieval. For February 1998, non-convergence was brought down from 11.4% to 4.3%, while the mean number of iteration steps (which dominates the computational time) dropped 8% from 5.15 to 4.76.

1 Introduction

There is a great need for information on the state and evolution of the global three-dimensional distribution of ozone in the atmosphere. Time series of ozone spanning years or even decades are important to detect changes in ozone which are coupled to climate change, and to monitor and understand the depletion and expected recovery of stratospheric ozone. Stratospheric ozone measurements are also used for operational numerical weather prediction models to constrain the energy balance in the stratosphere allowing improved forecasts. Knowledge on the distribution of ozone in the upper troposphere is important to quantify its contribution to radiative forcing and thus improve the understanding of climate change. Ozone in the boundary layer has adverse health effects and is an important species in air quality. Although boundary layer ozone is difficult to detect using the ultraviolet backscattered spectra measured from space, the inferred information on the tropospheric abundance is relevant for air quality modelling.

The key to retrieve the vertical distribution of ozone in the atmosphere from ultraviolet (UV) backscattered sunlight is the sharp decrease in the ozone absorption cross-section between 265 and 330 nm. Photons at the shortest wavelengths only penetrate the upper part of the atmosphere; therefore back-scattered short-wave photons contain information only of the upper layers of the atmosphere. Moving to longer wavelengths, deeper layers start to contribute to the back-scattered radiance. Beyond 300–310 nm (depending on the solar zenith angle) a sizeable fraction of the solar light reaches the surface. Combing the radiances over the whole wavelength range thus provides information of the ozone profile.

The Global Ozone Monitoring Experiment (GOME) was launched on the European Space Agency's second Earth Remote Sensing (ERS-2) satellite in April 1995 to measure backscattered ultraviolet (UV) and visible light at moderate spectral resolution (0.2–0.4 nm). To retrieve ozone profiles from its measurements in channels 1 and 2 (240–404 nm) several algorithms have been developed based on different techniques: optimal estimation (Barthia et al., 1996; Chance et al., 1997; Munro et al., 1998; Hoogen et al., 1999; Van der A et al., 2002), Philips-Tikhonov regularization (Hasekamp and Landgraf, 2001), and a neural network approach (Del Frate et al., 2002; Müller et al., 2003). An extensive intercomparison of these algorithms has been done by Meijer et al. (2006). Similar algorithms have also been applied to measurements from SBUV, SCIAMACHY, OMI and GOME-2.

At the Royal Netherlands Meteorological Institute (KNMI) the Ozone Profile Retrieval Algorithm (OPERA) (Van Oss and Spurr, 2002; Van der A et al., 2002) has been developed, based on the optimal estimation technique and able to ingest data from the satellite instruments GOME, GOME-2, and OMI. The quality of the OPERA retrievals from GOME data has been validated extensively by De Clerq et al. (2007) by comparing them with sonde, lidar, microwave and other satellite measurements. Since 2007, OPERA is used operationally for ozone profile retrievals from GOME-2 data in near real time.

In our study, we evaluate the global performance of the algorithm by its convergence behaviour. Bad convergence statistics indicates where the algorithm has problems to retrieve an ozone profile. In this way we can isolate geographical problem areas such as South America (Sect. 4) and deserts (Sect. 5). Studying the convergence statistics also allows us to assess the influence of the input data (such as the ozone cross section and the ozone climatology) on the retrieval result, as will be shown in Sects. 6 and 7. By implementing the algorithm adaptations and selecting better input data, the larger number of successful retrievals improves global coverage and increases average retrieval speed, facilitating the use of retrievals in near real time applications and the reprocessing of large datasets.

2 Algorithm overview and retrieval configuration

OPERA solves the inverse problem of retrieving the vertical ozone distribution from the measured radiance spectrum. In the forward step, it uses a radiative transfer model to calculate the spectrum from a model atmosphere including a first-guess ozone profile and estimates of cloud fraction and cloud height. The single scattering part of the radiation is computed with a fast single scattering model; the multiple scattering part is computed with the Linearized Discrete Ordinate Radiative Transfer model (LIDORTA) in four streams (Van Oss and Spurr, 2002), taking the sphericity of the atmosphere into account in the pseudo-spherical approximation. To limit calculation time, LIDORTA calculates scalar radiation fields. Polarization effects, which cannot be neglected (Hasekamp et al., 2002), are included afterwards by correcting with values from a look-up table that is created with the doubling-adding radiative transfer model which does include polarization (de Haan et al., 1987). In the inverse step, the difference between measured and simulated measurement is used to update the ozone profile and auxiliary parameters such as the effective surface albedo. The retrieval is ill-posed in the sense that many profiles give similar simulated spectra within given error bars. These profiles differ in their small-scale structures, which are not well constrained. By using the optimal estimation technique (Rodgers, 2000) an optimal solution is selected that combines information from the measurement with an a priori, climatological, ozone profile. Because of the non-linearity of the problem, an iteration scheme is needed, repeating the forward model and inverse step until certain convergence criteria are met on the solution (see below). Throughout this article the ozone climatology will be used to provide both the a priori for the optimal estimation and the first guess for the iteration.

In this paper we test the performance of our algorithm (OPERA version 1.0.9) with GOME data, taking advantage of the extensive calibration effort put into the measurements of this satellite instrument (Van der A et al., 2002; Krijger et al., 2005). Retrieval of ozone profiles requires absolutely calibrated reflectivities which makes it very sensitive to the accuracy and precision of the reflectivity calibration (van der A et al., 2002). Our results are based on the level 1b product extracted with the GOME Data Processor, version 4.01 (Slijkhuis, 2006), which contains corrections for the degradation of the reflectance, the radiance offset, and the polarization sensitivity. We restrict ourselves to data from 1998, i.e. before degradation of the sun-normalised radiance sets in.

Table 1 summarizes the most important retrieval settings and input data. The ozone profile is fitted for 40 atmospheric layers distributed homogeneously over altitude from surface level to 0.1 hPa. Furthermore, OPERA fits either the surface albedo or the cloud albedo, depending on the cloud fraction. Validation studies show that retrieval quality is improved further when OPERA fits a radiometric offset between measurement and simulated reflectance in the Band 1a window. Cloud fraction and cloud pressure are derived from the Oxygen-A band using the FRESCO algorithm (see Sect. 5).

3 Convergence criteria and global retrieval performance

Due to the non-linearity of the retrieval problem, the optimal estimation and its co-variance are calculated numerically by using an iteration scheme which is based on the Gauss-Newton method (Rodgers, 2000). This requires a convenient criterion for stopping the iteration. Here, we break off the iteration when the difference between the error-weighted lengths of two consecutive state vectors $\mathbf{S}_x^{-1/2}(\boldsymbol{x}_i - \boldsymbol{x}_{i+1})$ is below a fixed threshold ε:

$$(\boldsymbol{x}_i - \boldsymbol{x}_{i+1})^T \mathbf{S}_x^{-1} (\boldsymbol{x}_i - \boldsymbol{x}_{i+1}) < \varepsilon n$$

in which $\mathbf{S}_x$ indicates the covariance matrix of state vector $\boldsymbol{x}_i$, and n is the dimension of the "state space", the vector space spanned by the fit parameters. Throughout this study we will use ε=0.02. A stricter convergence criterion (e.g. taking ε=0.01) will slightly increase the mean iteration steps needed to reach convergence, but does not change the retrieval results significantly.

To investigate the algorithm behaviour for the full range of atmospheric and observational conditions, we use the algorithm with the default settings of Table 1 on a reference dataset of all retrievals in February 1998 (∼69 000 retrievals in orbit number 14557 to 14957, excluding narrow swaths). On average, 5.15 iteration steps were needed for convergence; 11.4% of the retrievals did not converge within 10 steps. As can be seen from the convergence statistics in Fig. 1, it is reasonable to break off the iteration after 10 steps when convergence criteria are still not met, since these retrieval apparently never converge.

We construct global monthly average fields of various parameters by projecting all GOME footprints on a grid of $1^{\circ} \times 1^{\circ}$. Figure 2a maps the mean number of iteration steps per grid cell, while Fig. 2b shows the mean fraction of not-converged retrievals;

a fraction of 1 indicates that for this grid cell all retrievals did not converge. In this way, different problem areas are uncovered. Apparently, the algorithm suffers from retrieval problems in distinct areas such as South America, deserts (such as Sahara and West Australia), Antarctic snow and ice. The band-like structure over the Pacific, roughly from Ecuador to Papua New Guinea, appears to correspond with the position of the intertropical convergence zone (ITCZ) for this month. These non-convergence issues will be addressed in the next sections. Furthermore, it will be shown that non-convergence can also originate from desert dust and from ozone anomalies.

The degrees of freedom for signal (DFS) is another useful measure to investigate the overall performance of the algorithm. Qualitatively, the DFS indicates how much information has been inferred from the measurements. If n is the dimension of the state space, we have DFS=n if the measurements completely determine the state vector, and DFS=0 if there is no information at all in the measurement, and the retrieval is completely determined by the a priori information. Typically, the DFS for the ozone profile fit parameters retrieved by OPERA for GOME measurements varies between 4 and 7, governed by the a priori errors, the measurements errors and the sensitivity of the radiation to the profile. The latter varies mainly with the solar zenith angle, the cloud fraction and the surface albedo.

4 South Atlantic anomaly

The area of non-convergence over South America in Fig. 2b corresponds with the location of the South Atlantic Anomaly (SAA). This is the region where the sun-synchronous satellite orbit (typically at 800 km altitude) intersects the inner Van Allen radiation belt. The high energetic particles (mainly protons and electrons) trapped inside this belt interact with the instrument, causing additional noise and spikes in the measurements. Due to the weak signal level at short wavelengths, especially radiance measurements in Band 1a are affected by the SAA (see Fig. 3). The distorted spectra can not be simulated by the radiative transfer model (RTM), and causes convergence problems for the algorithm.

In order to avoid this type of non-convergence, an SAA filter was implemented. Basically, it disqualifies all measurements from the Band-1a fit which are affected by the impact of high energetic particles. This is done by considering the reflectance R_{ref} at a certain wavelength λ_0 as a reference which is used to evaluate the validity of the neighbouring reflectance at the shorter wavelength side $R(\lambda_{i-1})$. This measurement is considered a statistical outlier and disqualified if its value is higher than R_{ref} plus n times the reflectance error σ:

$$R(\lambda_{i-1}) > R_{\mathrm{ref}} + n\sigma(\lambda_{i-1})$$

If not, $R(\lambda_{i-1})$ is taken as a new reference value to evaluate the next measurement. Note that we only test an upper boundary condition; testing for a lower boundary condition is not as straightforward due to the decreasing reflectance values towards shorter wavelengths.

Figure 4a shows the retrieval results for February 1998, using the SAA-filter with parameters λ_0=290 nm and n=3. By comparing with Fig. 2a, one can see that the SAA filter works well. For the region containing the SAA (here taken between 5° S–40° S latitude and 5° W–75° W longitude), the mean number of iteration steps is reduced from 7.51 to 6.90, mainly caused by a drop in non-convergence from 52.6% to 40.9%. Globally, non-convergence drops from 11.4% to 10.8% for this month.

The effectiveness and selectivity of the filter can be seen in Fig. 4b, which shows the mean number of spectral measurements used for the retrieval. Outside the SAA all measurements are used for retrieval; deep in the SAA the measurements become so noisy that almost all measurements in Band 1a are discarded: the total number of used measurements drops from 587 to 370. This causes the DFS to decrease, as can be seen in Fig. 4c.

5 Low cloud fractions at deserts

Since clouds in the field-of-view strongly affect the measured reflectance, they need to be included in the radiative simulation of the atmosphere. The convergence problems above deserts, as revealed by Fig. 2, can be related to the used cloud parameters. OPERA retrieves its cloud parameters by its in-built FRESCO algorithm, version 4 (see Koelemeijer et al., 2001). The effective cloud pressure P_c and the effective cloud fraction f_c are derived from the reflectivities in the oxygen-A band (758–766 nm), based on the principle that clouds screen the oxygen below the cloud. In the continuum the reflectivity depends mainly on the cloud fraction, the cloud albedo (here assumed to be 0.8) and the surface albedo (taken from a monthly global minimum-reflectivity database (Fournier et al., 2006). The depth of the absorption band, however, depends also on the cloud pressure.

The cloud parameters are used by the RTM, which performs two calculations: one cloud-free (R_{clear}) and one fully clouded (R_{cloud}) with clouds at pressure level P_c. The reflectance for the partially cloudy scene is computed from $R = f_c\, R_{\mathrm{cloud}} + (1 - f_c)\, R_{\mathrm{clear}}$ for each wavelength.

Depending on the cloud fraction, either surface or cloud albedo is included in the state vector. For $f_c \geq 0.2$, backscattered radiation is dominated by the bright clouds: OPERA will fit the cloud albedo and takes the surface albedo from a database. For $f_c < 0.2$ backscattered radiation from the surface becomes dominant, and OPERA will fit the surface albedo and sets the cloud albedo at 0.8.

The majority of convergence problems over deserts is caused by a surface albedo which is fitted to negative values. FRESCO overestimates small cloud fractions (see Fournier et al., 2006), because its minimum-reflectivity surface albedo database is not sufficiently decontaminated from the presence of absorbing desert dust aerosols and is therefore too low. The overestimated cloud fraction results in a simulated spectrum in which radiances are too high. In order to match the measured spectrum, the inverse step will lower the surface albedo. Because the initial surface albedo is small (typically

0.05 in the UV spectrum) and negative values are not allowed, there is not enough flexibility to compensate for the difference in radiance: the algorithm will not converge.

To prevent this problem, the following workaround has been implemented: if FRESCO retrieves $f_c < 0.2$ and in one of the consecutive iterations the surface albedo is fitted below zero, then f_c is set to 0 and the retrieval process is restarted. By doing so, the presence of clouds will be compensated by adjustments in the surface reflectance.

Although restarting to clear sky conditions takes at least one RTM-inversion cycle more, overall computation time is gained by avoiding non-convergence. Compared with Fig. 4a, Fig. 5a shows the improvement of retrieval results above deserts; global non-convergence statistics drop from 10.8% to 6.5%. The selectivity of this workaround is shown in Fig. 5b by mapping for each location the fraction of retrievals to which it has been applied. As can be easily seen, it applies mainly to desert areas, especially Sahara and Australia, but also the Namibian and Atacama desert and dry, sparsely clouded areas in Mexico and India.

The workaround also solves the convergence problem due to a dust outbreak event in February 1998 flowing out from West Africa towards South America; as a comparison Fig. 5c shows the mean aerosol optical depth at 500 nm for the same month. FRESCO attributes the increased reflectance (around 750 nm) due to the presence of the dust cloud over a dark ocean to an increased effective cloud fraction. The same dust cloud absorbs radiation in UV, lowering the reflectance measured in this regime. These two effects will force OPERA to retrieve the surface albedo below zero, which can be avoided by assuming a cloud-free model atmosphere.

To investigate the impact of the error which is introduced by neglecting a small cloud fraction, we select a representative not-converging desert pixel, the centre of its footprint 900 km west from Lake Chad, with cloud parameters f_c=0.105 and P_c=824 hPa according to FRESCO. We perform a set of retrievals for this pixel with P_c fixed at 824 hPa and f_c ranging from 0 to 0.2. Figure 6a shows the dependence of the retrieved ozone column and the surface albedo on the cloud fraction: overestimation of the real cloud fraction is compensated by a darker surface and more absorbing ozone. For

$f_c > 0.07$, the retrieved surface albedo becomes negative. Assuming a realistic surface albedo of 0.05 for our pixel we estimate the true cloud fraction to be f_c=0.025. In Fig. 6b all retrievals are plotted; absolute deviations from the reference retrieval at f_c=0.025 are shown in Fig. 5c. By switching to a cloud fraction of 0, the retrieved surface albedo increases to unrealistic high values (0.08 in our example). The retrieved total ozone column, however, decreases with less than 0.2%. This decrease is caused by a decrease in partial ozone column of the lower model layers up to 17 km; above the ozone bulk the profile doesn't change significantly.

6 Ozone cross-sections

Another important quantity that determines the accuracy of the radiative transfer calculation is the ozone absorption cross-section at vacuum. In OPERA, cross-section values are calculated from a lookup table, which is parameterized by wavelength and temperature. Errors in the used cross-sections can change the total retrieved ozone and the vertical distribution of this ozone significantly, as shown by Liu et al. (2007). Wrong cross-sections introduce an additional forward model error which influences the convergence statistics of the algorithm.

Here, we compare cross-sections from Bass-Pauer (abbreviated BP) (Bass and Pauer; Pauer and Bass, 1985) and Brion (abbreviated BR) (Brion et al., 1993; Daumont et al., 1992; Malicet et al., 1995). For both cross-sections the wavelengths have been converted to vacuum wavelengths (see e.g. Orphal and Chance, 2003); temperature dependence is described by a second order polynomial fit. BP compares with BR to within ~1% for wavelengths between 289–307 nm and temperatures between 209–278 K. For 326–337 nm however, the mean BP cross-sections are higher by 1–2% than BR (Liu et al., 2007).

Switching from BP to BR ozone cross-sections improves the convergence statistics of the retrieval algorithm considerably: for February 1998 the non-convergence drops from 6.5% to 5.0% (compare Fig. 5a with 8a), while the mean number of iteration steps reduces from 5.01 to 4.99.

To investigate whether this improved convergence affects the retrieval quality we validate the retrievals with ground measurements. A comprehensive validation study of OPERA retrievals (though based on an older algorithm version) has been done by De Clerq et al. (2007). Here, we restrict ourselves to 95 collocated microwave measurements (within 2 h and 400 km) done in Bern in 1998 with the GROMOS instrument (Dumitru, 2006). We prefer microwave above balloon sonde measurements for its ample altitude range (15–75 km compared to 0–30 km, respectively) and above lidar measurements for its short time interval between satellite overpass and ground measurement (0–2 h compared to 8–12 h).

GROMOS, operated since 1994 as part of the Network for the Detection of Stratospheric Change (NDSC), retrieves the ozone profiles using the optimal estimation method. Between 20–70 km the contribution of a priori profiles is less than 10% (Dumitru, 2006). The altitude resolution varies between 10–12 km at 30 km altitude level and 20–25 km at altitude levels above 60 km.

Figure 7 shows the validation results for retrievals performed with BP and with BR, compared with their corresponding microwave profiles which are smoothed with the averaging kernels from the retrieval method. For all retrievals the relative difference for each atmospheric layer is shown, together with the mean and the standard deviation. Errors in the forward model or model parameters show up as biases of the mean values. From Fig. 7 it can be seen that the GOME profiles correspond well with the microwave profiles in the mesosphere and around the ozone bulk at 10 hPa. In between the OPERA retrievals show an underestimation of ~5% for both cross sections, in correspondence with the validation study by De Clerq et al. (2007). Below the bulk, between 40–100 hPa, retrievals with BR underestimates the amount of ozone, while BP overestimates ozone in this range.

Due to the lower values of the BR cross-sections, the algorithm puts more ozone in its model atmosphere to compensate for the loss of absorbed radiance. The mean retrieved total ozone column in February 1998 therefore increases from 343 DU to

AMTD
3, 1163–1196, 2010
Improved ozone profile retrieval
B. Mijling et al.

346 DU (considering only retrievals which converge for both cross-sections), which is in accordance with the findings of Liu (2007). Compared with BP, BR cross sections cause the average profile to increase 14 DU in the 1000–100 hPa range and to decrease 12 DU in the 100–20 hPa range.

7 Ozone climatologies

In OPERA, the ozone climatology is used to select an ozone profile at the latitude and time of retrieval which serves both as a priori information and the initial state for the state vector. Ozone retrieval algorithms based on optimal estimation benefit from an accurate a priori in altitude regions where the measurement is less sensitive to the presence of ozone since the retrieval tends to the a priori in that case. Furthermore, it offers a convenient starting point for the iteration, taking the initial state vector close to the assumed true state. To study the effect of the ozone climatology on the retrieval behaviour, we performed retrievals for GOME measurements of February and October 1998, using three different ozone climatologies. To get optimal performance, the algorithm was set to use the SAA filter, the low cloud fractions work-around, and the BR cross sections.

7.1 Fortuin and Kelder

The Fortuin and Kelder (FK) climatology (see Fortuin and Kelder, 1998) is based on measurements of 30 ozone sonde stations between 1980–1991, covering the appearance of the ozone hole period but excluding the Pinatubo eruption. It describes the monthly mean ozone volume mixing ration for 17 zonal bands, ranging from 80° S to 80° N, at 19 pressure levels. The sonde measurements (from surface up to 10 hPa) are extended with the SBUV-SBUV/2 climatology (described in Randel and Wu, 1995) from 30–0.3 hPa. The standard deviation used here is the natural variability of ozone at each zonal band and at each pressure level for a certain month (Fortuin, 1996). For FK

AMTD

3, 1163–1196, 2010

Improved ozone profile retrieval

B. Mijling et al.

this is given up to 10 hPa; for higher atmospheric layers, OPERA extrapolates the error towards 0 at the top level. These standard deviations σ_i determine the diagonal elements of the a priori covariance matrix $\mathbf{S}_\mathrm{a}$. To allow for cross-correlations, off-diagonal elements are calculated using

$$[\mathbf{S}_\mathrm{a}]_{ij} = \exp\left(-\frac{|\log P_i - \log P_j|}{d}\right)\sigma_i\sigma_j$$

in which d is the ozone profile correlation length per pressure decade, here taken 0.5.

7.2 McPeters, Labow, and Logan

The climatology by McPeters, Labow, and Logan (MLL) (see McPeters et al., 2007) is also based on sonde measurements (1998–2002) for the troposphere, but is merged with SAGE II measurements (1999–2002) for the higher atmosphere. MLS data (1991–1999) is used at high latitudes where SAGE data is not available. MLL describes the monthly mean ozone mixing ratio and its standard deviation for 18 latitude intervals of 10 degrees on 61 altitude levels (0–60 km). As for FK, OPERA constructs the covariance matrix with a correlation length of 0.5.

7.3 TOMS version 8

The TOMS version 8 ozone climatology (TOMS) (Frith et al., 2004) describes the monthly partial columns for 11 atmospheric layers for 18 zonal bands. In addition, it includes the total ozone column as an extra parameter to select the most appropriate profile when the total column is known. This prevents problems at ozone anomalies such as in the ozone hole where the real profile differs too much from the monthly averaged profile. The dependence on total ozone is exploited in OPERA by using a fast algorithm for a total ozone column estimate, which is used to select the appropriate profile from the TOMS climatology.

To make a fast estimation of the total ozone column, we implemented the Temperature Independent Differential Absorption Spectroscopy (TIDAS) algorithm by Zehner (2002). The principle of TIDAS is to use the difference of reflectance ΔR at two wavelengths λ_1 and λ_2. By selecting λ_1=325.944 nm and λ_2=326.746 nm for the GOME instrument, a compromise is made in which broadband spectral features can be neglected and ΔR is relatively insensitive to the temperature dependence of the ozone cross section, the influence of the Ring effect, and interfering trace gas species such as NO_2, ClO_2, SO_2 and BrO. ΔR becomes proportional to the ozone slant column and with help of a geometric air mass factor the total column can be estimated.

Comparisons of the TIDAS estimates with the vertically integrated column values retrieved by OPERA show an agreement within 8% for the latitude range of -60° to $+60^\circ$. For higher latitudes, the difference can increase to 11%, but the TIDAS estimate is still appropriate for our purpose: selecting an a priori and initial profile from the climatology based on the estimated total column.

The TOMS climatology does not contain error estimation, and has to be postulated. Small errors express confidence in the a priori, resulting in good convergence but a low degree of freedom. Large errors put more weight to the measurements, resulting in a high DFS, but poor convergence. The FK and MLL climatologies typically have a relative error of ~15% for altitudes within and above the ozone bulk, and ~25% in the troposphere. Between 80 and 300 hPa the relative error increase to 30–50% to describe the variability in the altitude of the base of the ozone bulk. Because the base of the ozone bulk is better constrained when an ozone profile is selected based on its total column, there is less need for increased error estimates in this range. We find a good compromise by taking a fixed relative error between 15–25% for all layers, months and latitudes, and constructing the covariance matrix as in FK and MLL.

7.4 Intercomparison

To study the impact of different ozone climatologies on the retrieval, we focus on convergence behaviour and the degrees of freedom of the retrieval. Convergence

AMTD
3, 1163–1196, 2010

problems may arise when the a priori is not representative (either in shape, total ozone column value, or error) for the actual ozone distribution, or when the initial state vector is taken too far away from the true state.

Figure 8 shows the mean number of iteration steps for February and October 1998 (~78 000 retrievals in orbit number 18021 to 18464; excluding narrow swath) for the FK, MLL and TOMS climatology. As can be seen, the FK and MLL climatology give rise to important retrieval problems above Northern Europe in February and in the ozone hole in October. In both situations the climatology deviates too much from the truth, overestimating the total ozone column up to 70 DU for Northern Europe in February, and even more for the ozone hole. As a consequence, the retrieval needs more iteration steps, or does not converge at all. Because the TOMS climatology uses an a priori profile with a corresponding total ozone column, it offers a more accurate profile in these anomalous situations, which facilitates convergence here.

The left panels in Fig. 8 also reveal convergence problems around the equator related to the ITCZ in February 1998, especially for FK and MLL. The powerful convection in the ITCZ gives rise to a strong gradient in ozone concentrations between the bulk of the ozone and the very small concentrations in the troposphere. Here, the retrieval typically tends towards negative values for tropospheric atmospheric layers. Apparently, the real ozone distribution is better described by the TOMS climatology, resulting in better convergence. In October 1998 the retrieval problems due to the ITCZ are less pronounced for all three climatologies.

The convergence statistics and the mean DFS for February and October 1998 are summarized in Table 2. To give a representative value, the mean DFS is calculated for latitudes between 60° S and 60° N only, excluding the SAA. The convergence statistics for October 1998 with FK and MLL are dominated by the ozone hole region. Because in the ozone hole the algorithm performs better with TOMS (taking an a priori profile close to the real situation), global non-convergence drops from ~9% to ~4%. For February, convergence with TOMS at 15% error is comparable to MLL, and TOMS at 25% error is comparable to FK. All TOMS climatologies result in retrievals with a mean

DFS significantly better than retrievals done with MLL.

Figure 9 shows the zonal behaviour of the DFS for the different climatologies. For both February and October, retrievals with MLL have the lowest DFS, due to its small error estimate. Retrievals with TOMS at 25% error have the highest DFS. The drop in DFS below 60° S in October 1998 is due to the ozone hole. The few retrievals done with FK and MLL which do converge here are based on an a priori with a large error, showing therefore a sharp increase in DFS.

The choice of an ozone climatology depends on the application of the algorithm. TOMS at 15% is a good option when calculation speed is crucial, for instance in near real time applications. It has about the same fraction of successful retrievals as MLL, but at a higher DFS. Furthermore, it suffers less from retrieval problems at ozone anomalies. TOMS at 25% has the highest DFS, and can therefore be used in less time-critical applications were a maximum of information from the measurements is appreciated, such as in the processing of data assimilated time series.

8 Discussion and conclusion

Studying its convergence behaviour is an appropriate way to test the global performance of an ozone profile retrieval algorithm. Here we applied the OPERA algorithm on GOME measurements, taking advantage of the calibration effort done for the spectral measurements of this instrument. By taking data from 1998 we avoid degradation issues which affects GOME data of more recent years.

The convergence statistics for February and October uncover different classes of retrieval problems related e.g. to the South Atlantic Anomaly, low cloud fractions over deserts, desert dust outflow over the ocean, the intertropical convergence zone and ozone anomalies such as the ozone hole.

An algorithm adaptation has been implemented to filter out spiky measurements in the South Atlantic Anomaly region. The filter is selective, affecting predominantly measurements within the SAA. The convergence statistics improve for the SAA area, at the cost of loss of DFS. More elaborate SAA filter schemes can be implemented, but should always consider the balance between gain of speed and loss of information.

Problems with small clouds fractions above deserts can be avoided by neglecting clouds and switching to clear sky retrieval. The hereby introduced errors are acceptable (a decrease of ozone in tropospheric layers cause the total ozone column to reduce ∼1%). The workaround is selective and mainly affects desert areas like Sahara and Australia, and fixes retrieval problems at desert dust clouds above oceans. Switching to the new FRESCO+ cloud algorithm (Wang, 2006) in the OPERA software could also improve retrieval results above deserts. By taking Rayleigh scattering in the atmosphere into account, the global average of the retrieved cloud fraction becomes 0.01 lower. Clouds levels also drop, depending on cloud fractions (e.g. 100 hPa at f_c=0.2). Both effects will decrease the shielding of ozone by clouds in the atmosphere model. The simulated radiance at the top of atmosphere will decrease, reducing the mismatch between simulation and measurement.

Using Brion ozone cross-sections instead of Bass-Pauer cross-sections strongly reduces the non-convergence of the algorithm. Validation with the microwave measurements in Bern shows that retrievals done with BR are comparable with retrievals done with BP. For both cross-sections the retrieved profiles show an underestimation of ∼5% in the upper stratosphere. BR cross-sections, however, tend to reduce ozone in the lower part of the ozone bulk by shifting it to the troposphere and lower stratosphere.

The selection of ozone climatology in the optimal estimation method (here used as a priori and as initial state vector) importantly influences the retrieval results, such as convergence statistics, total column, profile shape, retrieval error, and DFS. We investigated this influence by comparing retrievals done with Fortuin and Kelder, McPeters and Labow, and the TOMS version 8 climatologies.

Both FK and MLL cause convergence problems at ozone anomalies (such as low ozone concentrations above Northern Europe in February 1998 and the ozone hole event of October 1998) which are not accurately enough described by the climatology. These problems are avoided with the TOMS climatology, which has the total ozone column as an extra parameter to select a suitable a priori ozone profile. Implementation of the TIDAS algorithm gives a quick estimate of the total column, accurate within 8% for the -60° to 60° latitude range. The TOMS climatology does not include an error estimate, but by postulating a relative error of 20% its retrievals have higher DFS and comparable or better convergence characteristics than both FK and MLL. The TOMS climatology also prevents convergence problems related to the ITCZ, which profiles apparently describe better the sharp gradient between tropospheric and ozone bulk in the ITCZ. The results with TOMS can be further improved by using an improved TOMS climatology, such as by Lamsal (2004), which solves some discontinuity issues over latitude, and includes a more realistic standard deviation, allowing for larger variability in the troposphere.

By implementing these algorithm improvements, more valid profile retrievals can be achieved in less computational time. For February 1998, non-convergence was brought down from 11.4% to 5.0% using FK climatology, or even further to 4.3% when using TOMS version 8 climatology with a fixed relative error of 20%. The computational time is dominated by the number of iteration steps, which in February on average dropped from 5.15 to 4.99 for FK, and down to 4.76 for TOMS.

Acknowledgements. The authors wish to thank the Institute of Applied Physics, University of Bern, Switzerland, for the use of their microwave ozone profile data and ESA for supplying the GOME level 1 data.

References

Bass, A. M. and Pauer, R. J.: The ultraviolet cross-sections of ozone, I. The measurements, in: Atmospheric Ozone, edited by: Zerefos, C. S., Ghazi, A., and Reidel, D., Norwell, Mass., 606–610, 1985.

Bhartia, P. K., McPeters, R. D., Mateer, C. L., Flynn, L. E., and Wellemeyer, C.: Algorithm for the estimation of vertical ozone profiles from the backscattered ultraviolet technique, J. Geophys. Res., 101, 18793–18806, 1996.

Brion, J., Chakir, A., Daumont, D., and Malicet, J.: High-resolution laboratory absorption cross section of O3. Temperature effect, Chem. Phys. Lett., 213(5–6), 610–512, 1993.
Brion, J., Chakir, A., Charbonnier, J., Daumont, D., Parisse, C., and Malicet, J.: Absorption spectra measurements for the ozone molecule in the 350–830 nm region, J. Atmos. Chem., 30, 291–299, 1998.
Chance, K. V., Burrows, J. P., Perner, D., and Schneider, W.: Satellite measurements of atmospheric ozone profiles, including tropospheric ozone, from ultraviolet/visible measurements in the nadir geometry: A potential method to retrieve tropospheric ozone, J. Quant. Spectrosc. Radiat. Transfer, 57(4), 467–476, 1997.
Daumont, M., Brion, J., Charbonnier, J., and Malicet, J.: Ozone UV spectroscopy I: Absorption cross-sections at room temperature, J. Atmos. Chem., 15, 145–155, 1992.
De Clercq, C., Lambert, J.-C., Granville, J., Gerard, P., Kaifel, A., Kaptur, J., Mijling, B., Tuinder, O., van Oss, R., and Zehner, C.: Geophysical information content and validation of ERS-2 GOME ozone profile data records, IASB-BIRA Technical Note TN-IASB-GOME1-CHEOPS-01-1/B, Issue 1, Rev. B, 123 pp., 20 December 2007.
De Haan, J. F., Bosma, P. B., and Hovenier, J. W.: The adding method for multiple scattering computations of polarized light, Astron. Astrophys., 183, 371–391, 1987.
Del Frate, F., Ortenzi, A., Casadio, S., and Zehner, C.: Application of neural algorithms for a real-time estimation of ozone profiles from GOME measurements, IEEE Trans. Geosci. Remote Sens., 40, 2263–2270, 2002.
Dumitru, M. C., Hocke, K., Kämpfer, N., and Calisesi, Y.: Comparison and validation studies related to ground-base microwave observations of ozone in the stratosphere and mesosphere, J. Atmos. Solar-Terr. Phys., 68(7), 745–756, 2006.
Fortuin, J. P. F.: An ozone climatology based on ozone sonde measurements, KNMI scientific report, WR 96-07, 1996.
Fortuin, J. P. F. and Kelder, H.: An ozone climatology based on ozone sonde and satellite measurements, J. Geophys. Res., 103(D24), 31709–31734, 1998.
Frith, S., Stolarski, R., and Bhartia, P. K.: Implications of Version 8 TOMS and SBUV Data for Long-term Trend Analysis, Proceedings of the XX Quadrennial Ozone Symposium, 1–8 June 2004, Kos, Greece, volume I, p. 65–66, The climatology data can be downloaded at http://jwocky.gsfc.nasa.gov/version8/version8_update.html, 2004.
Fournier, N., Stammes, P., de Graaf, M., van der A, R., Piters, A., Grzegorski, M., and Kokhanovsky, A.: Improving cloud information over deserts from SCIAMACHY Oxygen A-

band measurements, Atmos. Chem. Phys., 6, 163–172, 2006, http://www.atmos-chem-phys.net/6/163/2006/.

Hasekamp, O. P. and Landgraf, J.: Ozone profile retrieval from backscattered ultraviolet radiances: The inverse problem solved by regularization, J. Geophys. Res., 106, 8077–8088, 2001.

Hasekamp, O. P., Landgraf, J., and van Oss, R.: The need of polarization modeling for ozone profile retrieval from backscattered sunlight, J. Geophys. Res., 107(D23), 4692, doi:10.1029/2002JD002387, 2002.

Herman, J. R. and Celarier, E. A.: Earth surface reflectivity climatology at 340–380 nm from TOMS data, J. Geophys. Res., 102(D23), 28003–28012, doi:10.1029/97JD02074, 1997.

Hoogen, R., Rozanov, V., and Burrows, J. P.: Ozone profiles from GOME satellite data: Algorithm description and first validation, J. Geophys. Res., 104, 8263–8280, 1999.

Krijger, J. M., Aben, I., Landgraf, J.: CHEOPS-GOME: WP2.1: Study of Instrument Degradation, SRON-EOS/RP/05-018, 2005.

Koelemeijer, R. B. A., Stammes, P., Hovenier, J. W., and de Haan, J. F.: A fast method for retrieval of cloud parameters using oxygen A band measurements from the Global Ozone Monitoring Experiment, J. Geophys. Res. 106, 3475–3490, 2001.

Lamsal, L. N., Weber, M., Tellmann, S., and Burrows, J. P.: Ozone column classified climatology of ozone and temperature profiles based on ozonesonde and satellite data, J. Geophys. Res., 109, D20304, doi:10.1029/2004/JD004680, 2004.

Liu, X., Chance, K., Sioris, C. E., and Kurosu, T. P.: Impact of using different ozone cross sections on ozone profile retrievals from Global Ozone Monitoring Experiment (GOME) ultraviolet measurements, Atmos. Chem. Phys., 7, 3571–3578, 2007, http://www.atmos-chem-phys.net/7/3571/2007/.

Malicet, C., Daumont, D., Charbonnier, J., Parisse, C., Chakir, A., and Brion, J.: Ozone UV spectroscopy, II. Absorption cross-sections and temperature dependence, J. Atmos. Chem., 21, 263–273, 1995.

McPeters, R. D., Labow, G. J., and Logan, J. A.: Ozone climatological profiles for satellite retrieval algorithms, J. Geophys. Res., 112, D05308, doi:10.1029/2005JD006823, 2007.

Meijer, Y. J., Swart, D. P. J., Baier, F., Bhartia, P. K., Bodeker, G. E., Casadio, S., Chance, K., Del Frate, F., Erbertseder, T., Felder, M. D., Flynn, L. E., Godin-Beekmann, S., Hansen, G., Hasekamp, O. P., Kaifel, A., Kelder, H. M., Kerridge, B. J., Lambert, J.-C., Landgraf, J., Latter, B., Liu, X., McDermid, I. S., Pachepsky, Y., Rozanov, V., Siddans, R., Tellmann, S., van der

A, R. J., van Oss, R. F., Weber, M., and Zehner, C.: Evaluation of Global Ozone Monitoring Experiment (GOME) ozone profiles from nine different algorithms, J. Geophys. Res., 111, D21306, doi:10.1029/2005JD006778, 2006.
Müller, M. D., Kaifel, A. K., Weber, M., Tellmann, S., Burrows, J. P., and Loyola, D.: Ozone profile retrieval from Global Ozone Monitoring Experiment (GOME) data using a neural network approach (Neural Network Ozone Retrieval System (NNORSY)), J. Geophys. Res., 108(D16), 4497, doi:10.1029/2002JD002784, 2003.
Munro, R., Siddans, R., Reburn, W. J., and Kerridge, B. J. K.: Direct measurement of tropospheric ozone distributions from space, Nature, 392, 168–171, 1998.
Orphal, J. and Chance, K.: Ultraviolet and visible absorption cross-sections for HITRAN, J. Quant. Spectrosc. Radiat. Transfer, 82, 491–504, 2003.
Pauer, R. J. and Bass, A. M.: The ultraviolet cross-sections of ozone, II. Results and temperature dependence, in: Atmospheric Ozone, edited by: Zerefos, C. S., Ghazi, A., and Reidel, D., Norwell, Mass., 606–610, 1985.
Randel, J. W. and Wu, F.: Climatology of stratospheric ozone based on SBUV and SBUV/2 data: 1978–1994, NCAR/TN-412+STR, 137 pp., 1995.
Rodgers, C. D.: Inverse methods for atmospheric sounding, World Scientific Publishing Pte Ltd, New York, 2000.
Slijkhuis, S.: CHEOPS-GOME Algorithm Theoretical Basis Document Level 0 to 1 processing update, DLR report CH-TN-DLR-GO-0003, June 2006.
Uppala, S. M., Kållberg, P. W., Simmons, A. J., Andrae, U., da Costa Bechtold, V., Fiorino, M., Gibson, J. K., Haseler, J., Hernandez, A., Kelly, G. A., Li, X., Onogi, K., Saarinen, S., Sokka, N., Allan, R. P., Andersson, E., Arpe, K., Balmaseda, M. A., Beljaars, A. C. M., van de Berg, L., Bidlot, J., Bormann, N., Caires, S., Chevallier, F., Dethof, A., Dragosavac, M., Fisher, M., Fuentes, M., Hagemann, S., Hólm, E., Hoskins, B. J., Isaksen, L., Janssen, P. A. E. M., Jenne, R., McNally, A. P., Mahfouf, J.-F., Morcrette, J.-J., Rayner, N. A., Saunders, R. W., Simon, P., Sterl, A., Trenberth, K. E., Untch, A., Vasiljevic, D., Viterbo, P., and Woollen, J.: The ERA-40 re-analysis, Q. J. Roy. Meteorol. Soc., 131, 2961–3012, doi:10.1256/qj.04.176, 2005.
van der A, R. J., van Oss, R. F., Piters, A. J. M., Fortuin, J. P. F., Meijer, Y. J., and Kelder, H. M.: Ozone profile retrieval from recalibrated Global Ozone Monitoring Experiment data, J. Geophys. Res., 107(D15), 4239, doi:10.1029/2001JD000696, 2002.
van Oss, R. F. and de Haan, J. F.: Algorithm Theoretical Basis Document for OPERA, Issue

1.1, CHEOPS/KNMI/ATBD/001, 17–20, 2004.
van Oss, R. F. and Spurr, R. J. D.: Fast and accurate 4 and 6 stream linearised discrete ordinate radiative transfer models for ozone profile remote sensing retrieval, J. Quant. Spectrosc. Radiat. Transfer, 75, 177–220, 2002.
Wang, P., Stammes, P., and Fournier, N.: Test and first validation of FRESCO+ (2006), Proceedings of SPIE volume 6362, Remote Sensing 2006, Stockholm, Sweden, 11–16 September 2006.
Zehner, C., Casadio, S., di Sarra, A., and Putz, E.: Temperature Independent Differential Absorption Spectroscopy (TIDAS) and Simplified Atmospheric Air Mass Factor (SAMF) Techniques for the Measurement of Total Ozone Content using GOME Data, Proceeding of ERS/ENVISAT Symposium, 16–20 October, Goteborg, Sweden, 2001.

Table 1. Overview of the retrieval settings and input data.

Retrieval algorithm	OPERA, version 1.0.9
Satellite data	– GOME data 1998; level 1b product extracted with GDP 3.0.2 – Pixel size 960 km (across track)×100 km (along) – Overpass time at 10:30 local solar time
Atmospheric model	– 40 layers between 41 fixed pressure levels from 1000 to 0.1 hPa, equidistant in height – ECMWF temperature profiles (ERA-40, see Uppala et al., 2005), interpolated to time and location of retrieval – No aerosols
Cloud parameters	cloud fraction and cloud pressure retrieved from oxygen-A band by FRESCO version 4. Cloud albedo fixed at 0.8
Forward model settings	– 40 layers between 41 fixed pressure levels from 1000 to 0.1 hPa – Multiple scattering by LIDORTA (4 streams) – Correction for inelastic rotational Raman scattering included
Fit parameters, state vector	– partial ozone columns for 40 atmospheric layers – surface albedo (for cloud fraction $<20\%$) or cloud albedo (for cloud fraction $\geq 20\%$) – additional radiance offset in Band 1a
Fitting windows	– Band 1a (265–307 nm before 8 June 1998; 265–283 nm afterwards) – Band 1b (308–313.5 nm before 8 June 1998; 282–313.5 nm afterwards). 8 pixels are co-added to match one Band 1a pixel – Band 2 (315–330 nm). 8 pixels are co-added to match one Band 1a pixel
Ozone climatology (a priori and initial profile)	Fortuin and Kelder (1995, 1998) (reference setting) or McPeters et al. (2007) or TOMS version 8 (Frith et al., 2004)
Ozone cross sections	Bass Pauer et al. (1985) (reference setting) or Brion et al. (1993)
Surface albedo	TOMS UV database for λ=360 nm (Herman, 1997)
Maximum nr of iterations	10

AMTD

3, 1163–1196, 2010

Improved ozone profile retrieval

B. Mijling et al.

Table 2. Convergence statistics and mean DFS for different climatologies.

climatology	February 1998			October 1998		
	Not converged	Nr of iter. steps	Mean DFS	Not converged	Nr of iter. steps	Mean DFS
FK	5.0%	4.99	5.56	9.5%	4.92	5.18
MLL	2.5%	4.75	5.25	8.2%	4.80	4.76
TOMS 15%	3.2%	4.62	5.40	3.8%	4.55	5.11
TOMS 20%	4.3%	4.76	5.75	4.1%	4.62	5.45
TOMS 25%	5.4%	4.90	6.03	4.4%	4.67	5.70

AMTD

3, 1163–1196, 2010

Improved ozone profile retrieval

B. Mijling et al.

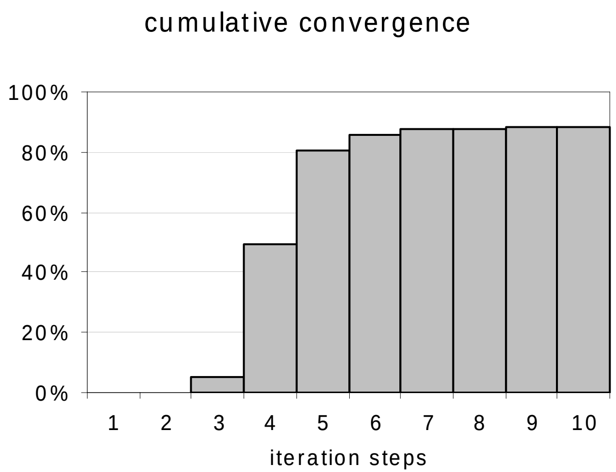

Fig. 1. Retrieval statistics for February 1998 with the settings of Table 1. 11.4% of the retrievals do not converge after 10 iteration steps.

AMTD
3, 1163–1196, 2010
Improved ozone profile retrieval
B. Mijling et al.

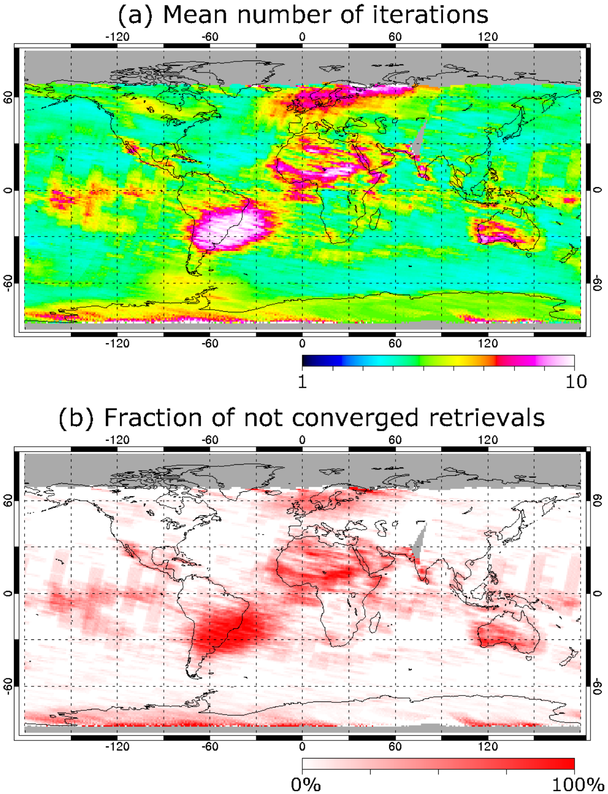

Fig. 2. **(a)** Mean number of iteration steps for all retrievals of February 1998. Non-converging retrievals are broken off after 10 iteration steps. **(b)** Fraction of not converged retrievals. Note the distinct areas of non-convergence.

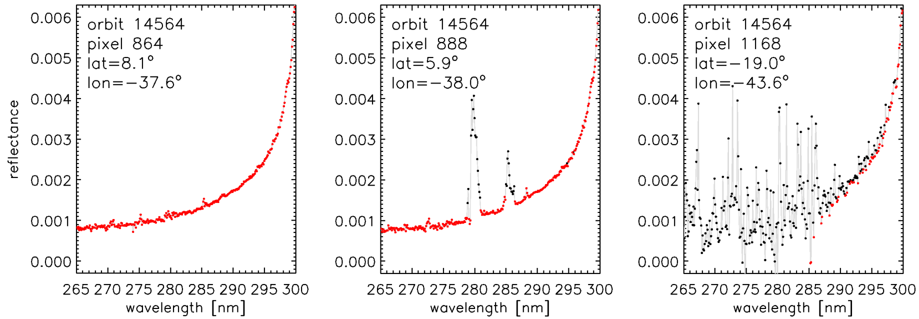

Fig. 3. Reflectance measurements in Band 1a for a typical measurement outside the SAA (left), on the edge of the SAA (middle), and in the center (right). Measurements which pass the filter are indicated by the red dots. Spikes and noisy parts of the measurements are blocked by the filter.

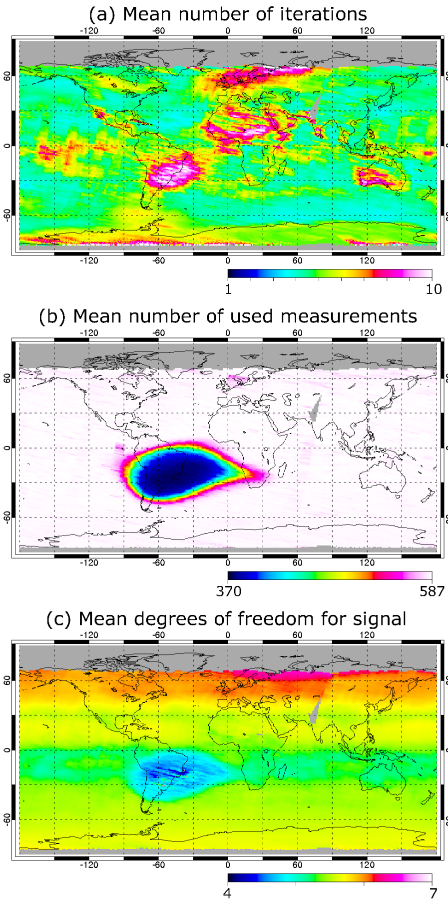

Fig. 4. Retrieval results for February 1998 with the SAA-filter applied. **(a)** Mean iteration steps. **(b)** Mean number of spectral measurements: only measurements in the SAA are affected by the filter. **(c)** The reduced number of measurements, however, results in a decrease of degrees of freedom for signal.

AMTD

3, 1163–1196, 2010

Improved ozone profile retrieval

B. Mijling et al.

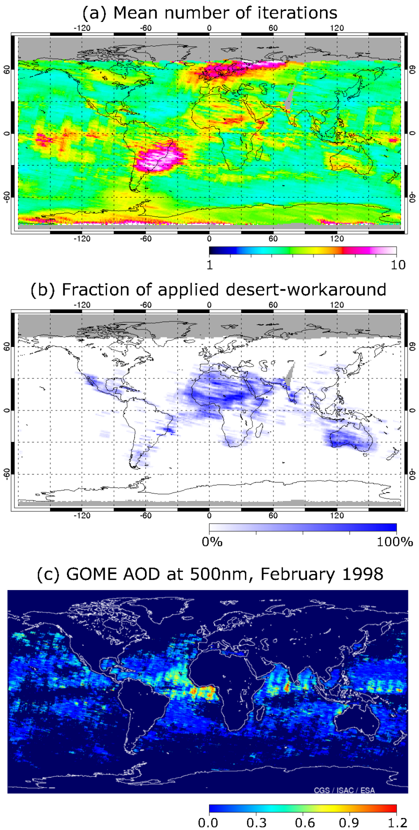

Fig. 5. Retrieval results for February 1998 with the desert workaround. **(a)** shows the improvement of retrieval results above deserts when compared with Fig. 4a; **(b)** shows the selectivity of the workaround by mapping for each grid cell the fraction of retrievals to which it has been applied. The convergence problem due to the dust outbreak flowing out from West Africa towards South America is also solved; as a comparison **(c)** shows the mean aerosol optical depth (AOD) at 500 nm for the same month (taken from http://www.temis.nl).

AMTD

3, 1163–1196, 2010

Title Page
Abstract | Introduction
Conclusions | References
Tables | Figures
◀| |▶
◀ ▶
Back | Close
Full Screen / Esc
Printer-friendly Version
Interactive Discussion

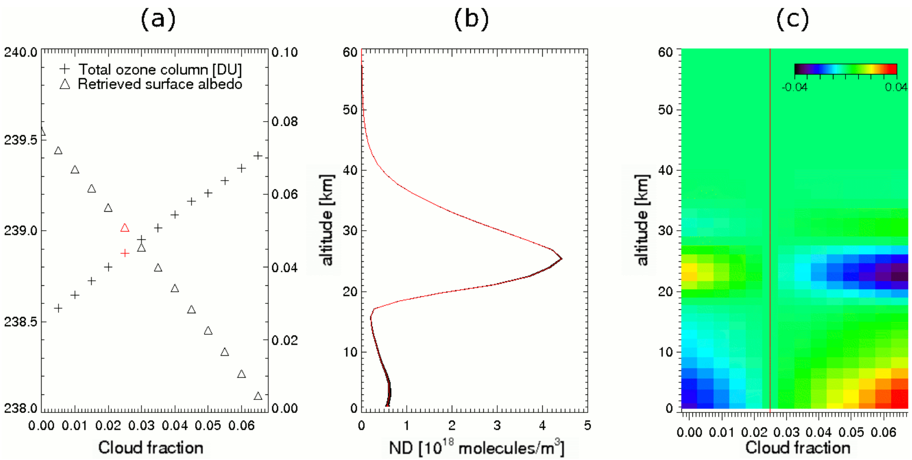

Fig. 6. **(a)** Dependence of retrieved surface albedo and total ozone column on the cloud fraction. In red, the retrieval corresponding to a surface albedo of 0.05, which is taken as a reference. **(b)** All retrieved ozone profiles. Small differences occur mainly in the lower part of the ozone bulk and in the troposphere. **(c)** shows the absolute deviation of number densities in 1018 molecules m^{-3} for each atmospheric layer with respect to the reference profile at f_c=0.025.

AMTD

3, 1163–1196, 2010

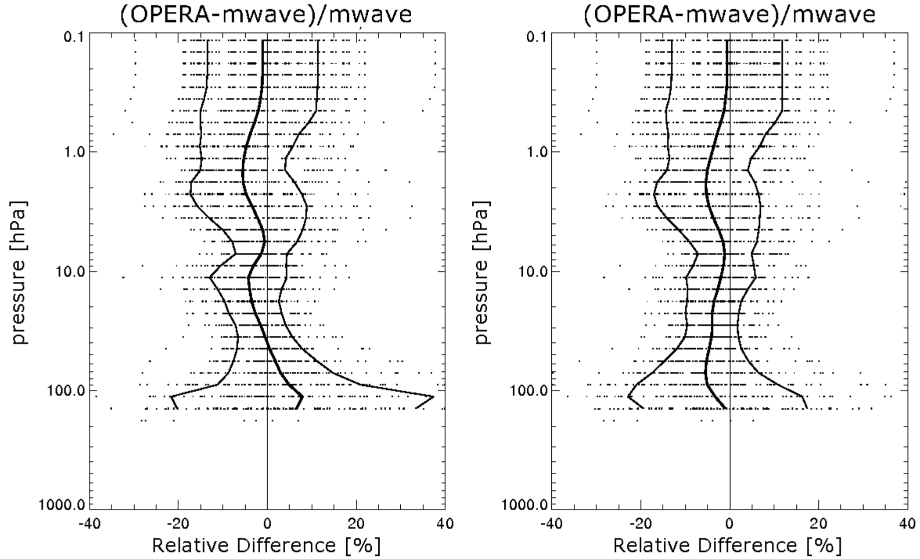

Fig. 7. Validation of 95 collocations (within 2 h and 400 km) of GOME retrievals with microwave measurements in Bern, 1998. The left panel shows the retrieval results done with Bass-Pauer ozone cross-sections, the right panel the results for Brion cross-sections. For each atmospheric layer the relative difference of the retrievals with the ground-based measurements is given, smoothed with the averaging kernel. The thick line connects the layer averages; the thin lines indicate the ±1 σ standard deviation.

AMTD

3, 1163–1196, 2010

Improved ozone profile retrieval

B. Mijling et al.

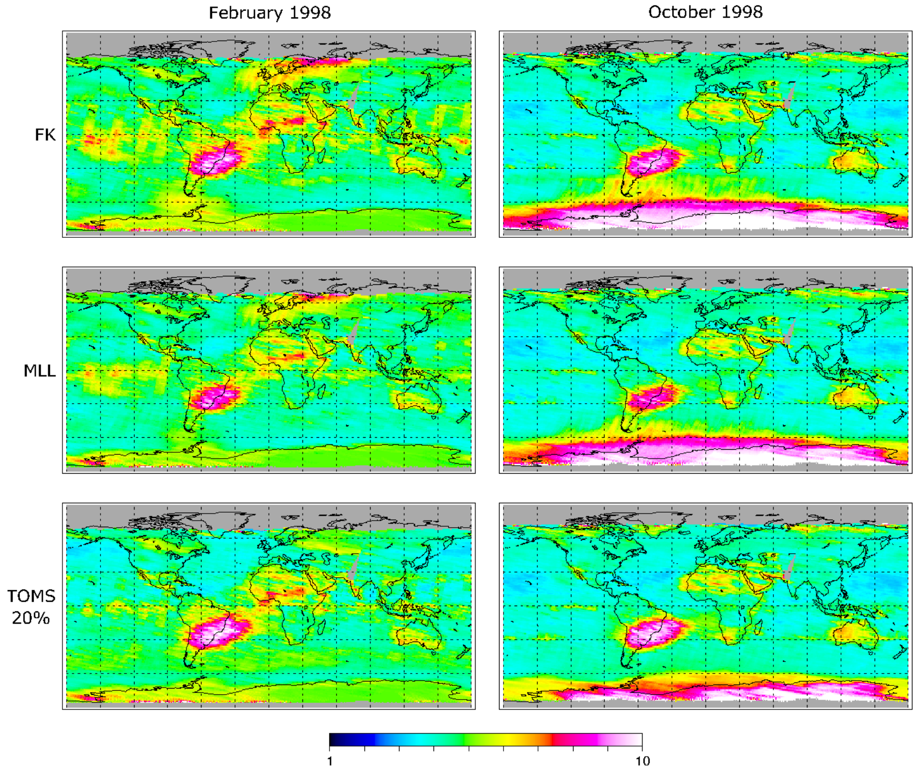

Fig. 8. Mean number of iterations for February 1998 (left panels) and October 1998 (right panels). In the rows the used ozone climatologies: FK, MLL and TOMS at a fixed relative error of 20%.

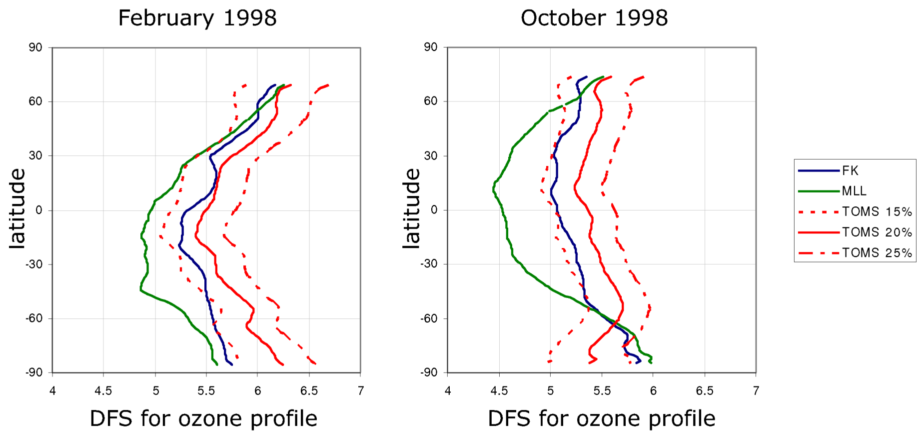

Fig. 9. Zonal mean degrees of freedom for signal for retrievals in February and October 1998, comparing different ozone climatologies: FK, MLL, and TOMS with relative errors at 15%, 17.5% and 20%. Only retrievals which converge in all climatologies are considered; the South Atlantic Anomaly was excluded from the calculation.